energies

MDPI

Article

Enhancement of the System Stability of DB-Controlled VSC Links Parallel Operated with a Weak Multi-Machine AC Power System

Liying Wang [1], Nesimi Ertugrul [2,*] and Michael Negnevitsky [3]

[1] AusNet Services, Melbourne 3006, Australia; liying.wang@ausnetservices.com.au
[2] School of Electrical and Electronic Engineering, University of Adelaide, Adelaide 5000, Australia
[3] School of Engineering and ICT, University of Tasmania, Hobart 7001, Australia; michael.negnevitsky@utas.edu.au
* Correspondence: nesimi.ertugrul@adelaide.edu.au

Abstract: To allow the large-scale integration of renewable energy sources into the grid, VSC-HVDC is commonly utilized. However, with greater integration, several power system stability issues arise. In this study, we examined the small-signal rotor angle stability of a model of the Australian power system with embedded VSC-based HVDC links. A simplified model of the Australian power network was used to connect the potential geothermal resources in the region of Innamincka using a 1100 km HVDC link. We observed that the introduction of the new source of geothermal power generation had an adverse impact on the damping performance of the system. Therefore, two forms of stabilization are examined here: (i) generator power system stabilizers (PSS) fitted to the synchronous machines, which are used to convert geothermal energy to electrical power; and (ii) power oscillation damping controllers (PODs) fitted to the VSC-HVDC link. In the case of the PODs, two types of stabilizing input signals are considered: (i) local signals such as power flow in adjacent AC lines, and (ii) wide-area signals such as bus voltage angles at key nodes in the various regions of the system. It was concluded that the small-signal rotor angle stability of the interconnected AC/DC system can be greatly enhanced by employing the designed damping controllers.

Keywords: power system stabilizer; power oscillation damping; wide-area power oscillation damping

check for updates

Citation: Wang, L.; Ertugrul, N.; Negnevitsky, M. Enhancement of the System Stability of DB-Controlled VSC Links Parallel Operated with a Weak Multi-Machine AC Power System. *Energies* **2022**, *15*, 2424. https://doi.org/10.3390/en15072424

Academic Editor: Alon Kuperman

Received: 6 March 2022
Accepted: 23 March 2022
Published: 25 March 2022

Publisher's Note: MDPI stays neutral with regard to jurisdictional claims in published maps and institutional affiliations.

Copyright: © 2022 by the authors. Licensee MDPI, Basel, Switzerland. This article is an open access article distributed under the terms and conditions of the Creative Commons Attribution (CC BY) license (https://creativecommons.org/licenses/by/4.0/).

1. Introduction

The applications of renewable energy resources such as wind and solar PV are growing as the ratio of conventional synchronous generators is diminishing. Although rapidly increasing renewable energy resources allow Australia to reach its zero carbon targets quickly, they bring significant network problems. A potential solution to this issue is to utilize rich geothermal resources in the northeast of South Australia (SA) as a zero-emission synchronous base-load generation. These geothermal reserves are primarily located around Innamincka in the Cooper Basin that is near the border between SA and Queensland. However, the integration of such a high-capacity renewable source at a significant distance from the shared transmission network is a difficult task. This is due to the fact that the Australian grid is one of the longest (more than 4000 km) and thinnest power networks in the world, spanning from Port Douglas of Queensland to Port Lincoln of South Australia [1]. Several pilot projects have already been studied to utilize these geothermal energy resources in the Australian power network [2–5]. However, in this paper, we propose a different approach, which can be defined as a more feasible and suitable power transmission strategy that employs the dead-beat (DB)-controlled voltage source converter-based high-voltage direct current (VSC-HVDC) links to interconnect the weak, multi-machine Australian power system.

Modern large, interconnected power systems are characterized by the requirements to transmit large amounts of power over long distances, large-scale integration of renewable energy resources, and deregulation of power system operations. These lead to the development of large hybrid AC/DC grid infrastructures.

The hybrid AC/DC grid is capable of enhancing the system stability by relieving the congestion and transmission bottlenecks and also acts as a firewall against cascade disturbances while preventing blackouts [6,7]. However, the integration of VSC-HVDC links with weak AC grids may deteriorate the damping of the inter-area modes [8,9]. In addition, the sub-synchronous resonance is a common problem, as the first adverse interaction between the turbine generator torsional modes of the vibration and a conventional HVDC transmission system was observed in the Square Butte Electric Coop Project in North Dakota [10] in 1977.

The solutions for enhancing the damping of electromechanical modes of oscillation in a power system can be divided into two major categories: (i) power system stabilizers (PSSs) fitted to synchronous generators [11] and (ii) power oscillation dampers (PODs) fitted to flexible AC transmission systems (FACTs) [12–16], HVDC links [7–9,17–21], and potentially asynchronous generators such as wind turbines [22]. As the VSC-HVDC is the primary research direction in this paper, the majority of the reviews have been performed on the HVDC damping controller.

It was reported in [9] that the VSC-HVDC link has four controllable quantities, within which the inter-area modes are able to be decoupled by two ΔPs and the local modes within the area where the converter located can be simultaneously damped by each ΔV (or ΔQ). However, it is investigated in [17] that active power control is more effective in damping electromechanical modes of oscillation than reactive power control. Therefore, in this paper, active power and the DC voltage are considered as the most suitable inputs to PODs fitted to VSC-HVDC links.

Furthermore, depending on whether the input signal to the POD is local or remote, it can be classified as (i) a local POD or (ii) a wide-area power oscillation damper (WAPOD). Due to the limitations in the signal communication, initially, the local POD is adopted. However, due to the developments in global position system (GPS) and satellite communication technology, the WAPOD is now technically feasible. Therefore, the combination of these two POD types are becoming important as power systems evolve [16].

The effectiveness of the POD design depends on the location of the controlled plant (relates to controllability), the modal content of the selected stabilizing signal (relates to observability), and the measurement accuracy of the selected signal. Two different approaches on feedback signal selection were investigated to damp out the inter-area mode in the Hydro-Quebec network [23], which were the geometric (also known as controllability/observability index) and the residue approaches. In the study, the geometric approach is found more reliable than the residue approach that is widely used. Moreover, the global signal input is found more effective than the local signal. However, it should be emphasized here that the performance of local POD and WAPOD depends on five major factors [16]: the actual tuning of those PODs, the availability of measurements with suitable "modal content", the power system configuration and disturbances, the location of VSC, and the specific operating point.

In [24], the Hankel singular value (HSV) approach is added to complete the comparison of controllability/observability and residue methods. It was concluded that in a small, two-area system, the residue and Hankel singular value methods performed in a similar way. However, in a medium-scale system, the system damping performance was better when signal selection was based on the HSV method. Furthermore, the design approaches of PSS and POD were investigated in [25–30].

Most recently, enhancing system stability through PODs were studied on the Hydro-Québec network [23], the Nordic power system [16], the reduced Great Britain model [31], the China Southern Power Grid (CSG) [32,33], and the New England test system integrated with the New York power system [21].

Utilization of PODs for damping inter-area modes of oscillation were also investigated in the Australian network. To stabilize the interconnection between NSW and Queensland [34], the PODs fitted to SVCs were investigated in [25,27], and the improvements in damping controls of the SVCs (based on local bus frequency measurements) were studied in [35]. However, the PODs in VSC-HVDC links in these three references presented three major limitations that constitute the focus of this paper. These limitations are:

- A single infinite bus is typically employed but is not sufficiently accurate.
- A simplified VSC-HVDC model is commonly adopted (also as in [36]).
- The proposed PSS/PODs are not validated over a range of operating points.

It should be noted here that there is a potential application of the paralleled VSC-HVDC link and the AC link to transmit power from the large geothermal sources from the regions mentioned before to the load centers. Therefore, the small-signal stability of the proposed system will be examined first, in which participation factor analysis of the critical mode is employed to evaluate the impacts of the new geothermal source. Secondly, the power system stabilizer will be designed and assessed to enhance the damping performance of the proposed AC/DC hybrid system.

The computer simulations were performed using the simplified and modified South Eastern (SE) Australian power network under different loading conditions. Therefore, the contributions of this paper, which are covered in the consecutive sections, can be summarized as follows.

(1) Studying the damping performance of the proposed PSS/POD over the full range of modal frequencies in the future Australian network;
(2) Application of the VSC-HVDCs utilizing the detailed model of damping controller;
(3) Modal analysis of the AC/DC hybrid grid to characterize different modes using participation factors; and
(4) Validation of the modal damping by the PSS/POD over a wide range of operating conditions.

2. Modeling of the Extended Australian Power System

2.1. Propose Transmission Scheme and Its Configuration

A simplified model of the Australian power network is used to integrate the potential geothermal resource of 2000 MW (see Figure 1). In the new network, it is assumed that 200 MW of power is consumed locally, and 1200 MW of power is delivered to the Armadale converter substation via a $\pm$500 kV and 1100 km transmission system with bi-pole VSC-HVDC links.

The Armadale converter substation is positioned halfway between Queensland and New South Wales, hence offering full utilization of the existing transmission corridor in both states. The remaining 600 MW of power is transferred to Roxby Down from Innamincka, using the 490 km 275 kV transmission line, and it is integrated into the main grid at Port Augusta by a 290 km transmission line. The major network modification is illustrated in Area 6 of Figure 1 with dashed lines.

The power network model in Figure 1 is modified based on an IEEE 14-generator, 59-bus system, which can offer a reliable platform for small-signal analysis or for the validation of the proposed PSS/PODs in a multi-machine system. It can be reported here that the original network model was composed of five areas in total, fourteen large generators, and five static var compensators (SVCs), as it is given in [37].

To create more oscillatory behavior of the system, it is assumed that fourteen generators are equipped with the power system stabilizers (PSSs) with an equivalent damping gain of 10 per unit, while only the three Innamincka machines are assumed to operate without PSSs. It should be noted that the original system is still stable under this assumption.

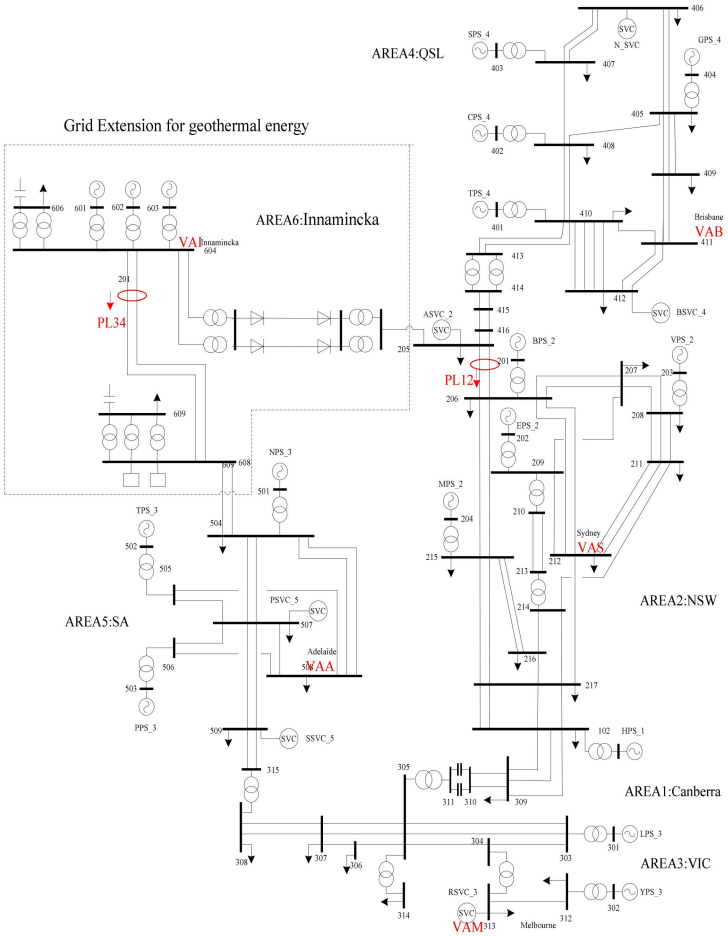

Figure 1. The diagram of the modified (with Area 6) South Eastern Australian power grid with VSC-HVDC links.

2.2. VSC-HVDC Model

In [38], a robust control scheme that is applicable to this research was reported, which is capable of operating with a weak AC grid where the minimum short-circuit ratio (SCR) is equal to 2 and is also able to operate over a wide range of operating points. A generalized small-signal modeling of voltage source converters with dead-beat current controllers was also given in [38]. Using the scaling technique and the DC link parameter sensitivity examination, the same control parameters as in these references are also used in the new VSC-HVDC links.

2.2.1. Scaling Technique

The procedure of scaling the system parameters is given in Figure 2. The scaling starts with the transfer of the original system values to per-unit values. Then, using Equation (1), they are converted back to the new SI units. Therefore, the developed VSC-HVDC link model that is designed for a particular system rating remains unchanged.

$$x^{(new)} = \frac{x^{(original)}}{x^{(original)}_{base}} \cdot x^{(new)}_{base} \tag{1}$$

The same technique is applicable to the inner current controller, PLL control, and all outer loop controllers. The methodology to verify the accuracy of the system scaling technique is developed as in Figures 3 and 4. The eigenvalue calculation of the original and scaled systems (Figure 5) reveals that the proposed scaling technique is effective.

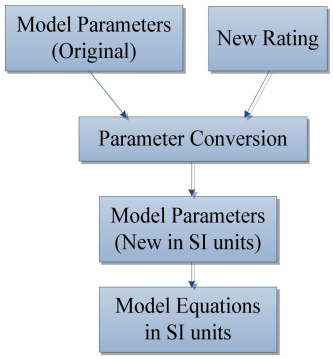

Figure 2. System parameter scaling scheme.

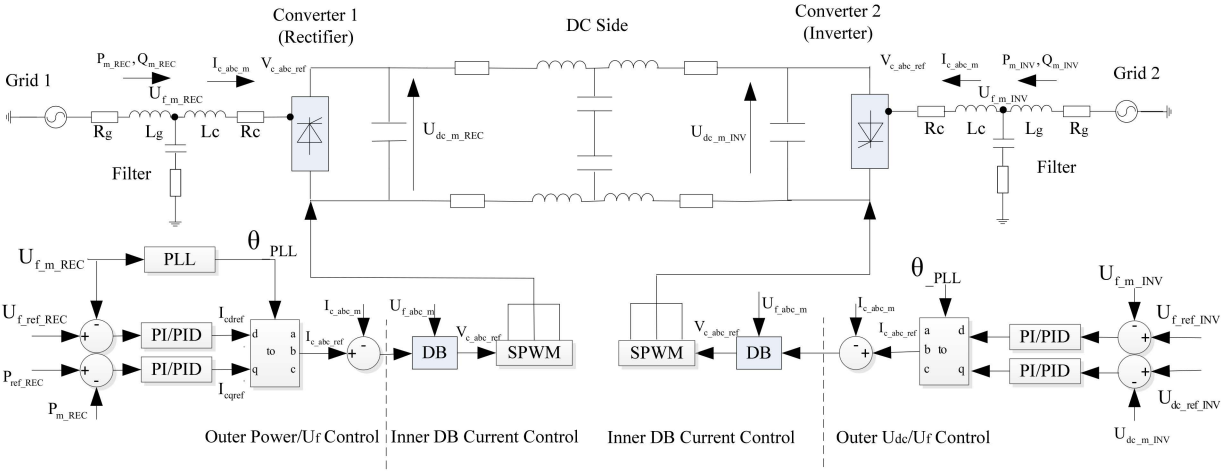

Figure 3. Overall control structure of a point-to-point VSC-HVDC link.

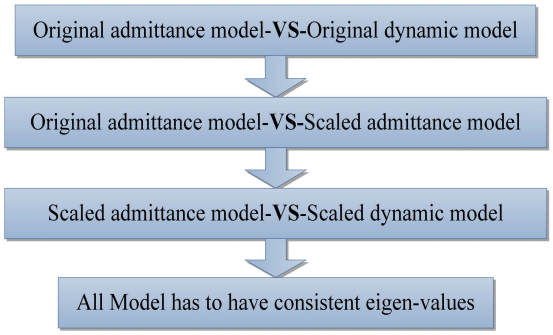

Figure 4. Flow chart of the verification methodology of modeling.

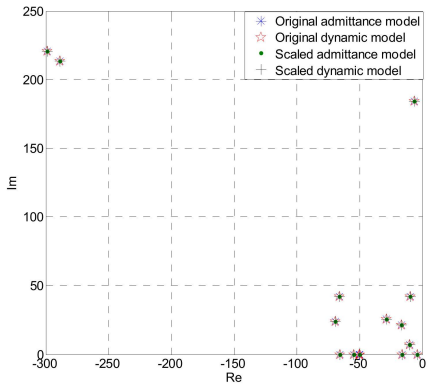

Figure 5. Eigenvalue map of the original and scaled systems, which indicate the identical values.

2.2.2. DC Link Parameter Sensitivity

As it is shown above, the modified models can be scaled to different ratings, but the DC link parameters cannot be scaled since the DC link is physically present. Therefore, the robustness and sensitivity of the designed controllers in [38] should be examined.

The HVDC link parameters utilized in this paper are obtained from the project reported in [39], which has a ±500 kV 1046 km transmission system at a power level of 1200 MW with line commutate converters (LCC) [40]. The parameters of a single line are R_{Link} = 26 Ω, L_{Link} = 0.46 H, and C_{link} = 13.73 μF. As it was also reported in [41], the transmission pole voltage considered in this research is realistic.

Figure 6 shows the eigenvalue map of the system with a new series of updated DC link parameters. It can be seen in the figure that there are significant changes in a pair of modes: 41.83 rad/s moves to 84.91 rad/s and 184 rad/s moves towards 569.2 rad/s. Therefore, it is critical to determine the impacts of this variation on the efficiency of the controllers designed. This is studied by evaluating the performance of all the power and voltage controllers using the new series of DC link parameters. It was concluded that no significant effects are observed on the controllers within the frequency range considered, which confirmed the robustness and sensitivity of the new controllers to the DC link parameters.

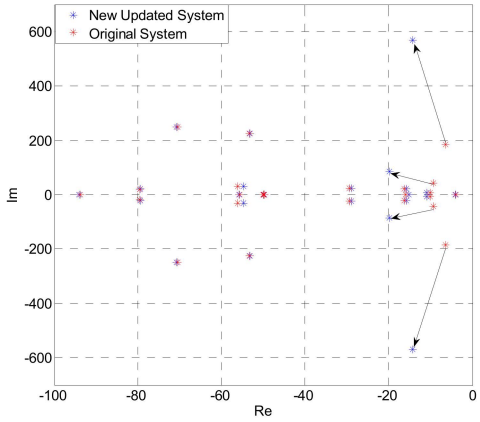

Figure 6. The comparison of the system eigenvalues between the new updated DC link system and the original system.

2.2.3. Admittance Matrix Representation of the Integrated Grid and Filter

In [38], to obtain high-accuracy VSC controllers, a dynamic model was utilized, which represents the interconnected simplified grid model. The model is represented by a source behind impedance or with additional resistance depending on the SCR and X/R ratios of the system. Nevertheless, the frequency range of interest in this study is the modal frequency related to electromechanical oscillations, which is more likely encountered in practice. The frequency range is reported in [37] varies from low-frequency inter-area mode of 1.5 rad/s to higher local frequencies of 12 rad/s. Therefore, it is necessary to test the validity of the interconnected grid and PCC bus filter as an admittance matrix within the frequency range of interest. It can be noted here that it is insufficient to employ the constant admittance representation of the grid for torsional oscillations in studies of HVDC interactions, since the frequency of interest in this application is much higher.

In [42], a "hybrid model" was also proposed to offer a feasible solution to the above problem. This was achieved by using the detailed model of the dynamics of the transmission network as well as the dynamic devices in adjacent area of HVDC converters. The other parts are modeled as constant admittances. It was found that this approach offers higher accuracy and simplicity. Therefore, the simplification process of the grid and filter dynamic model must be examined to validate the suitability of admittance matrix representation of the integrated grid and the filter.

Figure 7 illustrates the relationship of the system variables, where the grid and filter models are represented as admittances, which can be given by Equation (2). The simulation results in Figure 5 reveal that the further simplification of the filter model does not weaken the accuracy of the results in this application. Therefore, the admittance representation of both the grid and the filter models is the standard modeling methodology in the following analysis.

$$\begin{cases} \widehat{u}^g_f = \widehat{E}^g_g - Z_g \widehat{I}^g_g \\ \widehat{I}^g_g = \widehat{I}^g_f + \widehat{I}^g_c \\ \widehat{I}^g_f = \widehat{u}^g_f \cdot B_f j \end{cases} \tag{2}$$

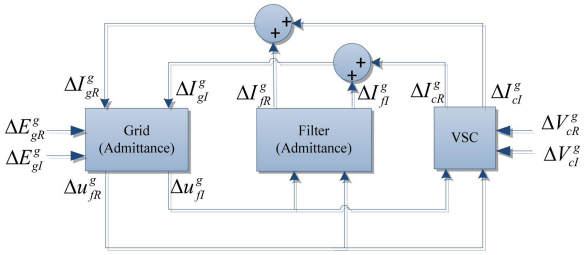

Figure 7. The grid and filter model as an admittance.

If the above equation is expanded and linearized, the small-signal model of the filter and grid admittance representation of the system model can be obtained as:

$$\begin{cases} \Delta u^g{}_{f_R} = E^g{}_{g_R} - R_g \Delta I^g{}_{g_R} + X_g \Delta I^g{}_{g_I} \\ \Delta u^g{}_{f_I} = E^g{}_{g_I} - R_g \Delta I^g{}_{g_I} - X_g \Delta I^g{}_{g_R} \end{cases} \tag{3}$$

$$\begin{cases} \Delta I^g{}_{g_R} = \Delta I^g{}_{f_R} + \Delta I^g{}_{c_R} \\ \Delta I^g{}_{g_I} = \Delta I^g{}_{f_I} + \Delta I^g{}_{c_I} \end{cases} \tag{4}$$

$$\begin{cases} \Delta I^g{}_{f_R} = -\Delta u^g{}_{f_I} \cdot B_f \\ \Delta I^g{}_{f_I} = \Delta u^g{}_{f_R} \cdot B_f \end{cases} \tag{5}$$

2.2.4. The Algorithm for Interconnection of the Sub-Systems

Once the state space models of the sub-systems have been defined, they are able to be grouped together to form a single set of state space model of the overall system by employing the interconnection algorithm presented in Appendix A. This can facilitate the application of the classic control theory for steady-state stability analysis and controller design.

3. The Identification of Electromechanical Damping Modes of the System

By conducting the eigenvalue analysis for the interconnected system, the inter-area modes are summarized in Table 1. The eigenvalue map of the main electromechanical modes of the interconnected system is given in Figure 8. The results indicate that the introduction of the new source of geothermal power generation has an adverse impact on the damping performance of the system since the main inter-area modes of I40, I35, I25, and I15 are lightly damped. The damping criterion used here is chosen according to the Australian National Electricity Rules, which require that the halving time of the least-damped electromechanical mode of oscillation should not be more than five seconds ($1/T \leq \ln(2)/5$) [1]. This corresponds to a damping constant with a magnitude greater than -0.14 (N_p/s), as it is highlighted in Figure 8. As it is also indicated, mode I15 is the least-damped inter-area mode. The fourth row of Table 1 indicates that the machines in Queensland oscillate against those in Innamincka, SA, and Victoria. In addition, the participation factor analysis results in Figure 9 suggest that the affecting factors can be used

to separate the machines into three groups: the machines at SA, approximately 7.58–10.7%; the Innamincka machines, about 6.71% each; and finally, the NPS machine in SA, the GPS machine and the SPS machine in Queensland, and the LPS machine in Victoria, ranging from 5.05% to 2.29%.

Table 1. Inter-area modes of the integrating system.

Mode	Case: Three Generators (Innamincka) with PSSs Out of Service			
	Real	**Imag.**	**Damping Ratio**	**Mode Description**
I 40	−0.286	3.907	0.073	Innamincka and VIC, and Canberra VS SA
I 35	−0.290	3.417	0.085	Innamincka VS VIC and SA
I 25	−0.242	2.273	0.106	Innamincka and SA and QLD VS VIC, NSW, and Canberra
I 15	−0.154	1.703	0.090	QLD VS Innamincka and SA, and VIC

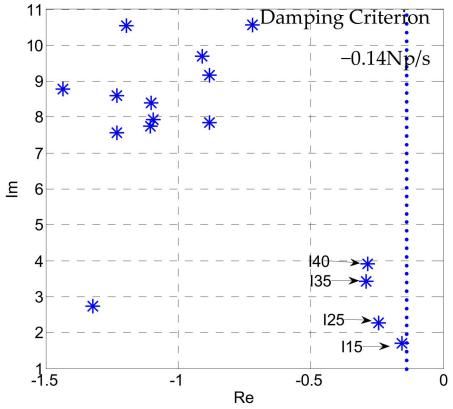

Figure 8. Eigenvalue map of the interconnected system.

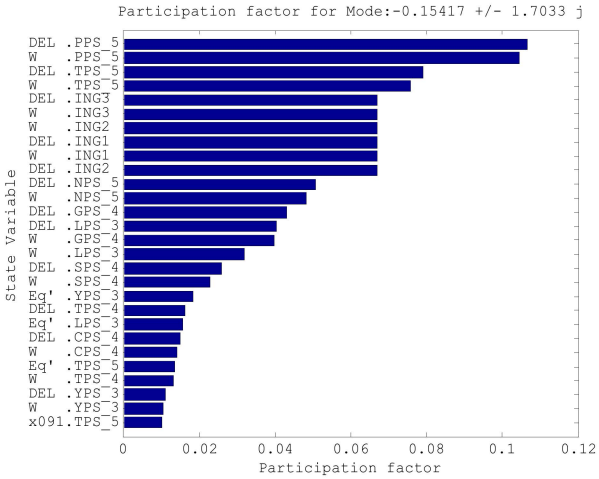

Figure 9. Participation factor for mode I15.

4. Supplementary Controllers Design

To enhance the damping performance of the target system, the PSS and PODs are designed as described below.

4.1. Local PSS Design and Assessment

4.1.1. PSS Design

The PSS design, which is also described in [26,43], involved the following steps:

Step 1: Determine the torque coefficients induced by PSS. In other words, specify the DAMP(s) coefficient and add the wash-out filter and low-pass filter to the coefficient to properly obtain the transfer function of the stabilizer DAMP(s).

Step 2: Obtain the gain and phase characteristic of the excitation system, the generator, and the power system (i.e., the PV_r characteristic).

Step 3: Apply curve fitting to the selected PV_r characteristic.

Step 4: Derive the PSS transfer function.

Step 5: Assess the performance of PSS by using eigenvalue analysis and comparing the torque coefficients induced by the PSS specified with the specified value.

Typically, *DAMP(s)* has the following form:

$$DAMP(s) = D_e \cdot B(s) \tag{6}$$

$$B(s) = \left(\frac{sT_w}{1+sT_w}\right)\left(\frac{1}{1+sT_p}\right)^N \tag{7}$$

In this case, the time constants for the wash-out filter and low-pass filter are 3 s and 0.05 s, respectively. Then, the transfer function of B(s) and *DAMP(s)* can be obtained easily.

To disable the shaft dynamics of all the machines, the transfer function from the voltage reference input (V_r) of the automatic voltage regulator (AVR) on Innamincka generator #1 to the torque of the electrical power output (P) that $PV_r(s)$ can be easily calculated, as shown in Figure 10 (solid blue line). For design purposes, the $PV_r(s)$ should be fitted to a lower-order plant, as given in Equation (12). Its corresponding Bode plot is given in Figure 10 (dotted red line).

$$PVr(s) = \frac{18.6s + 3268}{s^2 + 15.25s + 59.63} = 54.805 \cdot \frac{0.0056916s + 1}{0.01677s^2 + 0.25574s + 1} \tag{8}$$

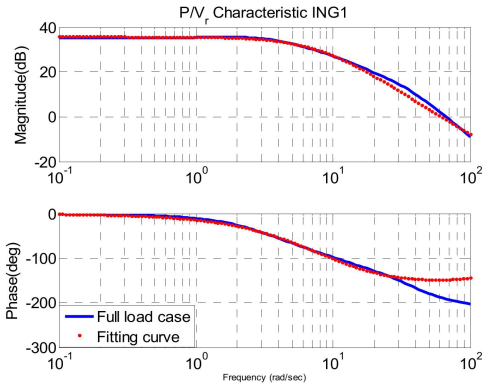

Figure 10. PVr characteristic and curve fitting for Innamincka generator #1.

Then, we convert PVr(s) from pu on S_{base} (100 MVA) to pu on M_{base} (750 MVA) and specify the *DAMP(s)* function as:

$$PVr_M(s) = K_{sm} \cdot G(s) = K_{sm} \cdot \frac{1 + 0.0056916s}{0.01677s^2 + 0.25574s + 1} \tag{9}$$

where $K_{sm} = K_s \cdot S_{base} / M_{base} = 54.805 \cdot 100/750 = 7.3073$.

The transfer function of PSS is that PSS(s) and the system PVr characteristics PVr(s) are related in terms of the following equation:

$$PSS(s) \cdot PVr(s) = DAMP(s) \tag{10}$$

Then, the PSS transfer function can be easily derived as:

$$\begin{aligned} PSS(s) &= DAMP(s)/PVr_M(s) \\ PSS(s) &= (D_{PSS}/K_{sm})\cdot(\tfrac{3s}{1+3s})\cdot(\tfrac{1}{1+0.05s})(\tfrac{0.01677s^2+0.25574s+1}{0.0056916s+1}) \\ PSS(s) &= (0.13685\cdot D_{PSS})\cdot(\tfrac{3s}{1+3s})\cdot(\tfrac{1}{1+0.05s})(\tfrac{0.01677s^2+0.25574s+1}{0.0056916s+1}) \end{aligned} \quad (11)$$

4.1.2. PSS Assessment

Figure 11a reveals that the damping performance of the system under the high loading condition has been enhanced by the designed PSS. However, it can be noted that the compensation added by PSS is not significant, and it can be further verified by conducting a small step test (0.01 pu) on the voltage reference of Innamincka generator #1 (see Figure 12). Figure 12 shows that the response of the generator output power is damped slightly by comparing the cases with (dashed black curve) and without PSS (solid red line). In addition, the damping performance of the system under the light loading condition has not been changed significantly, which can be verified by the eigenvalue map given in Figure 11b. As it can be seen in the figure, the eigenvalues of this operating mode have not been significantly left-shifted. However, this does not deteriorate the damping performance of the system (see Figure 12). To further improve the damping performance of the system, the damping torque is added by introducing supplementary POD controllers are necessary.

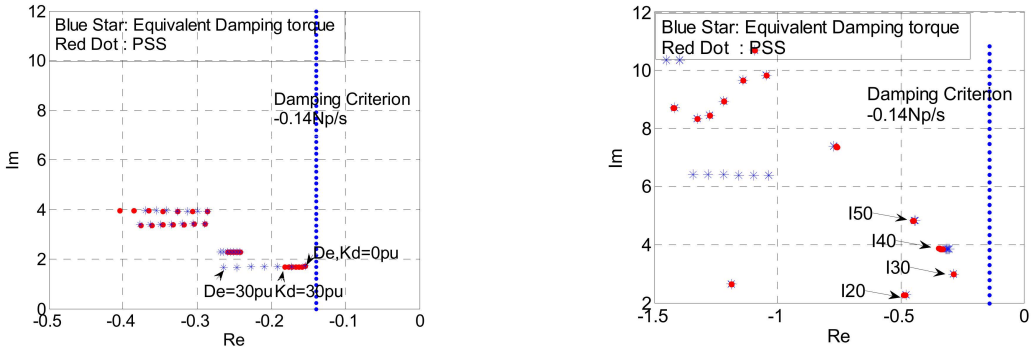

Figure 11. The comparison of the rotor modes of the system with the equivalent damping torque (blue star) and the system fitted with PSS (red dot) under the high loading condition and light loading condition. The damping gain in Innamincka generators increased from zero (no PSS in service) to 30 pu in 5 pu. (**a**) High loading condition; (**b**) Light loading condition.

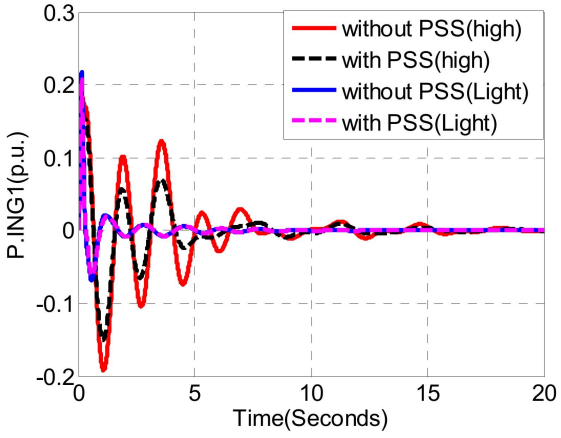

Figure 12. Comparison of the power output of generator #1 from Innamincka under the condition with and without PSS in service by applying a small disturbance of 0.01 pu on the reference voltage of Innamincka generator #1.

4.2. POD Design and Assessment

The auxiliary devices fitted to the FACTS devices for enhancing power system stability are called the power oscillation damping controllers, which are designed to enhance the damping performance of certain inter-area modes. Based on the source of the feedback signals, two types of POD, local POD and wide-area POD (WAPOD), are designed systematically based on the "residue" method. The residue analysis gives an indication of the selection of the best suitable feedback signal, which is the one with the largest residue, since such a signal is defined to be capable of improving the targeting oscillation mode with less effort [44].

Figure 13 shows the general structure of the AC/DC hybrid network with POD damping controllers. The POD controllers are composed of an amplification block, a wash-out and a low-pass filter, and m_c stages lead-lag blocks. The transfer function G(s) of the POD controllers can be given by:

$$G(s) = k \cdot \frac{1}{1+sT_{LP}} \cdot \frac{sT_w}{1+sT_w} \cdot \left[\frac{1+sT_{lead}}{1+sT_{lag}}\right]^{mc} \tag{12}$$

where T_{LP} denotes the time constant of the low-pass filter, T_w stands for the time constant of the wash-out filter, T_{lead} and T_{lag} imply time constants for the lead-lag block, and m_c is the number of compensation stages (usually m_c = 2).

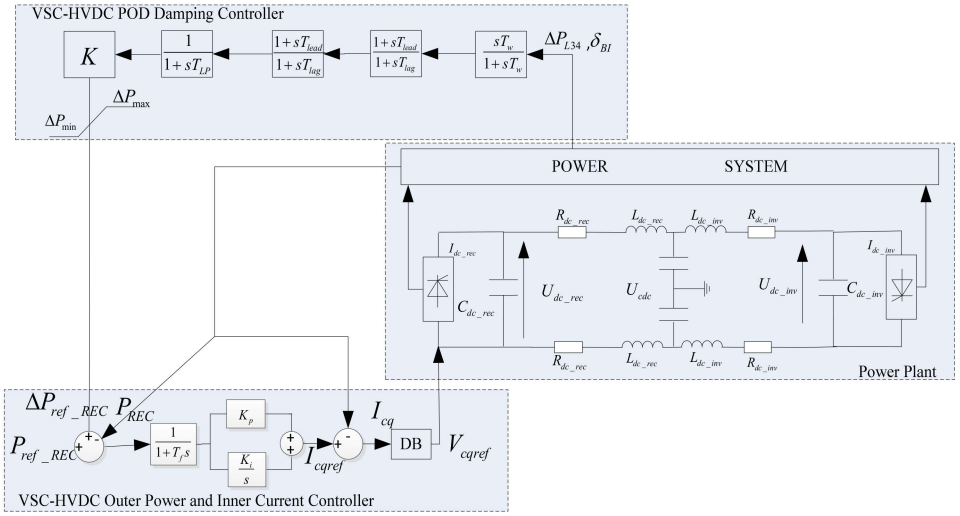

Figure 13. The schematic diagram of the VSC-HVDC damping system.

The theoretical analysis and the systematic design approaches are well documented in [25,27,44]. Assuming that the excitation mode of the system is the "target mode" λ_h only, the simplified approximate model of the target system can be given by $R_h/(s-\lambda_h)$, where R_h is the open-loop residue from the selected input to the output of the MIMO system for the particular h-th complex mode. Furthermore, assuming that the POD controller G(s) is in place, the closed-loop transfer function for the POD loop and the balanced equation for λ_h via the eigenvalue calculation can be obtained. Furthermore, by applying the small-signal technique and first-order Taylor series expansion, we can obtain the left shift of a "target mode" caused by the POD controllers that satisfies the below equation:

$$\Delta\lambda_h \approx k \cdot R_h \cdot G(\lambda_h) \tag{13}$$

where k is chosen such that:

$$k << 1/\left(R_h \cdot \left(\frac{\partial G(s)}{\partial s}\Big|_{s=\lambda_h}\right)\right) \tag{14}$$

In order to left-shift the target mode horizontally by using a POD controller as in Equation (16), the parameter selections of T_{lead} and T_{lag} must satisfy the following relationship [27]:

$$\varphi_{comp} = \arg(G(\lambda_h)) = 180^0 - \arg(R_h) \tag{15}$$

where for G(s),

$$\alpha_c = T_{lead}/T_{lag} = (1 - \sin(\frac{\varphi_{comp}}{m_c}))/(1 + \sin(\frac{\varphi_{comp}}{m_c})) \tag{16}$$

$$T_{lead} = 1/(\omega_i\sqrt{\alpha_c}); T_{lag} = \alpha_c \cdot T_{lag} \tag{17}$$

4.2.1. Residue Analysis

Table A1 presented in Appendix A shows the residue analysis for the interconnected system. For the local POD, the power flow in adjacent AC lines ΔP_{L34} is selected as the input signal since it has relatively higher residue [25]. For the same reason, the bus voltage angle difference between Brisbane and Innamincka, $\Delta\delta_{BI}$, is chosen as the input signal for the WAPOD.

In Table A1, 17 different modes and two types of stabilizing input signals are considered: (i) local signals such as power flow in adjacent AC lines (ΔP_{L12}, ΔP_{L34}) and (ii) wide-area signals such as bus voltage angles at key nodes (VAB, VAS, VAM, VAA, VAI) in the various regions of the system (refer to Figure 1). In Table A1, δ and ω denote the bus voltage angle and frequency, respectively, while the subscripts B, S, M, A, and I denote the five areas Brisbane, Sydney, Melbourne, Adelaide, and Innamincka, respectively.

4.2.2. Local POD Design

As it is given in Table A1, the residue angle from P_{REF_REC} to ΔP_{L34} under the least-damped mode I15 (at frequency of 1.7033 rad/s) is 89.684°. Using Equations (15)–(17), T_{lead} and T_{lag} can be calculated as 1.4229 s and 0.24224 s, respectively. Then, the transfer function of the local POD can be given by:

$$\begin{aligned} POD(s) &= KSS \cdot Q(s) \\ &= KSS \cdot (\tfrac{10s}{1+10s}) \cdot (\tfrac{1}{1+0.01s}) \cdot (\tfrac{1+1.4229s}{1+0.24224s})^2 \end{aligned} \tag{18}$$

The root locus analysis was conducted and the eigenvalue map of the system for different values of the amplification block KSS is shown in Figure 14. The target inter-area mode I15 is left-shifted from -0.1549 N_p/s to -0.3862 N_p/s under the high loading condition (see Figure 14a), which also resulted in shift of the inter-area modes of I40, I35, and I25. Mode I20 is shifted to the right, but still with a sufficient damping ratio. This is also the cause of the first swing appearing in the "with local POD only" plot in Figure 14. In addition, for the system under the light loading condition (Figure 14b), the modes I50, I30, and I25 remain unchanged, and mode I40 shifted but is still within the acceptable limit. Similar to the high loading condition, mode I20 is also shifted to the right, but with an adequate damping performance.

By comparing the eigenvalue maps of the system with the coefficient KSS varying from 3.642×10^{-3} to 7.03642×10^{-2} at a step size of 0.01, and with PSS on and off, it can be concluded that the inclusion of PSS has significantly improved the inter-area mode I40. However, the other three inter-area modes display small improvements under the heavy loading conditions (Figure 15a). For the system under the light loading condition, the predicted effects of PSS and POD can be observed in Figure 15b. No significant impact was observed after placing these damping controllers in service. Although the mode I40 slightly deteriorated, it remained within the acceptable limit.

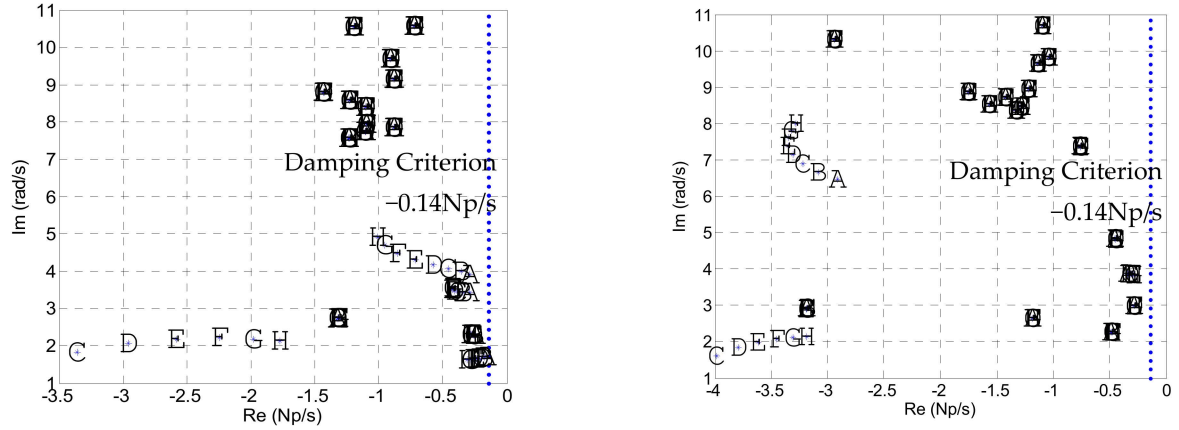

(**a**) (**b**)

Figure 14. The eigenvalue map of system fitted with POD, where the letters represent the gains of the POD, and KSS is increased from 3.642×10^{-3} to 7.03642×10^{-2} with a step size of 0.01. (**a**) High loading condition; (**b**) light loading condition.

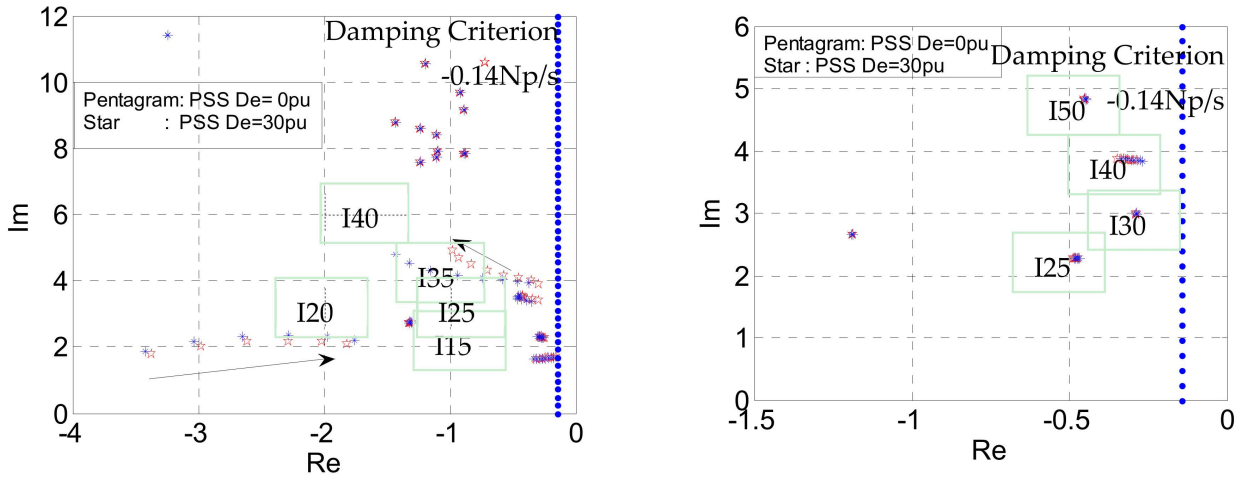

(**a**) (**b**)

Figure 15. The eigenvalue map of system fitted with POD and PSS. The letters are the gains of the POD, and KSS is increased from 3.642×10^{-3} to 7.03642×10^{-2} with a step size of 0.01. (**a**) High loading condition; (**b**) light loading condition.

By applying the small-signal disturbance test (0.01 pu on the reference voltage command) to Innamincka generator #1, the damping performance of the system is improved by placing the PSS and POD controller (see Figure 16). The plot labeled "with POD (Local) only" provides a better damping performance than "the PSS only" controller. However, all these supplementary control schemes can provide satisfactory improvements to damping the system inter-area modes.

4.2.3. Wide-Area POD Design

As displayed in the residue analysis in Table A1, the residue angle from P_{REF_REC} to $\Delta\delta_{BI}$ of the lightly damped mode I15 is 70.661°. Similarly, for the WAPOD, the results of the calculated T_{lead} and T_{lag} are 1.8435 s and 0.18697 s, respectively. The transfer function for the WAPOD can be obtained by:

$$POD(s) = KSS \cdot Q(s) = KSS \cdot \left(\frac{10s}{1+10s}\right) \cdot \left(\frac{1}{1+0.01s}\right) \left(\frac{1+1.8435s}{1+0.18697s}\right)^2 \quad (19)$$

By increasing the amplification block coefficients KSS from 3.642×10^{-3} to 0.12 with a step size of 0.02, the eigenvalue evolution map was obtained by conducting the root locus analysis, as given in Figures 17 and 18. The results in Figure 17 indicate a significant improvement in the damping performances of all four inter-area modes under the high loading condition. To examine the system sensitivity to the employment of WAPOD (designed to improve the damping performance of the high loading condition), the damping performance of the light loading condition is also tested.

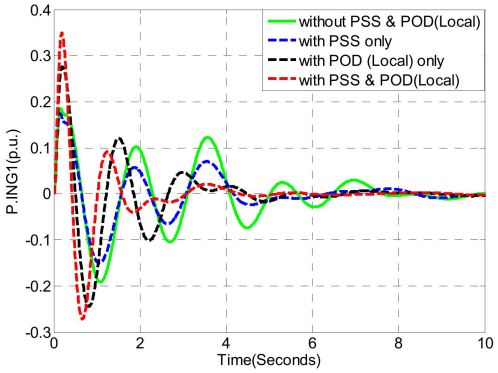

Figure 16. Power output of Innamincka generator #1 following a 0.01 pu step change on the voltage reference of Innamincka generators.

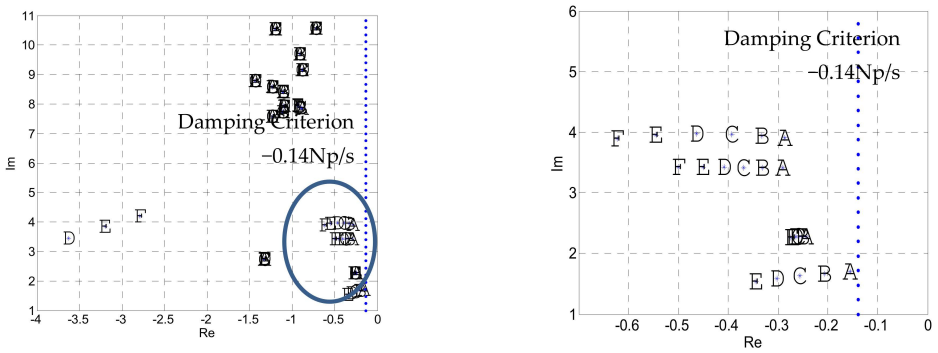

(**a**) (**b**)

Figure 17. The eigenvalue map of the system fitted with WAPOD under high loading condition, where the letters represent the gains of the WAPOD, as KSS is increased from 3.642×10^{-4} to 0.12 with a step size of 0.02. (**a**) High loading condition; (**b**) zoomed-in version of the above figure (circled area).

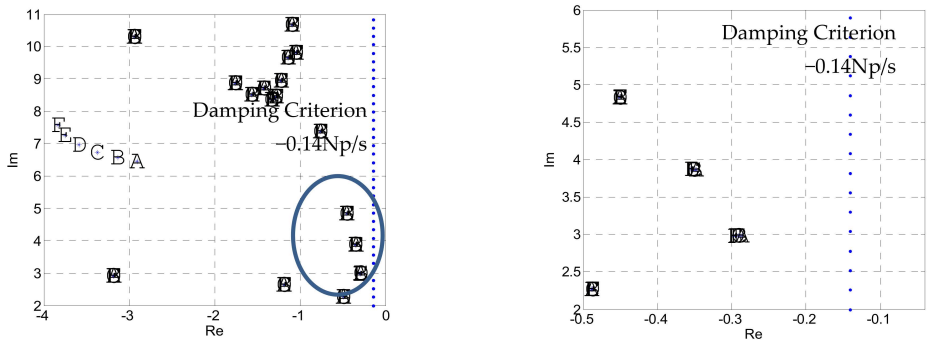

(**a**) (**b**)

Figure 18. The eigenvalue map of the system fitted with WAPOD under light loading condition, where the letters represent the gains of the WAPOD, while KSS is increased from 3.642×10^{-4} to 0.12 with a step size of 0.02. (**a**) Light loading condition; (**b**) zoomed-in version of the above figure (circled area).

The simulation results suggest that using WAPOD does not deteriorate the light loading scenario, but it does not significantly improve it, either (see Figure 18).

Figure 19 shows the eigenvalue analysis of the system operating under the high loading condition by employing the WAPOD damping controller and the PSS controller. It can be observed from the figure that the damping performance of the system improved significantly when employing the PSS only. This is further confirmed by the time response plot shown in Figure 20, which demonstrates that the adequate damping performance can be solely obtained by the WAPOD controller in service. In addition, it is shown that the performance of WAPOD together with PSS is better than that of local POD with PSS controller (red curve and magenta curve in Figure 20).

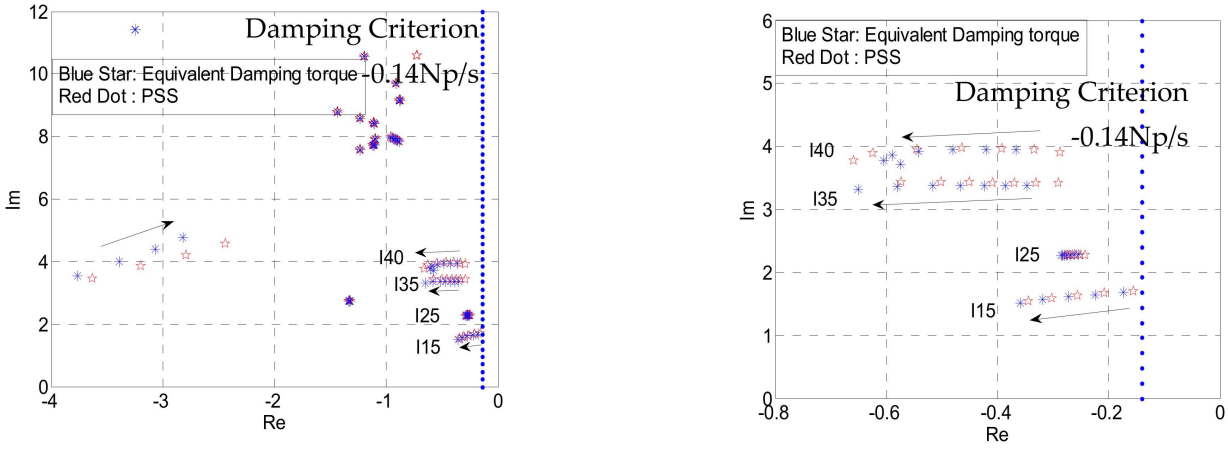

(**a**) (**b**)

Figure 19. Eigenvalue analysis of WAPOD with PSS under high loading condition, where KSS is increased from 3.642×10^{-4} to 0.12 with a step size of 0.02. (**a**) High loading condition; (**b**) zoomed-in version of Figure 19a (circled area).

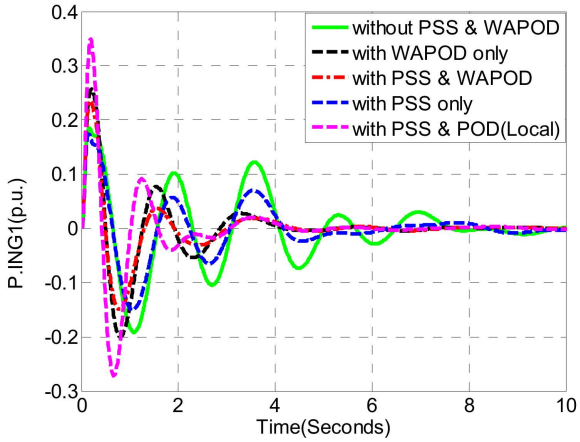

Figure 20. Power outputs of Innamincka generator #1 following a step change of 0.01 pu on voltage reference of Innamincka generators.

The oscillating curves of "with PSS&POD (Local)" in Figures 16 and 20 have larger first cycles compared with the results presented in Figure 12. This is an acceptable result. Although the designed controller serves to improve the damping performance of the active power response, the target process aims to achieve an energy balance in a transient timeframe when the power system is subject to a small-signal disturbance. Therefore, to decrease the halving time of the active power response (i.e., improving the damping performance of the active power controller), the magnitude of the first cycle response must increase.

5. Conclusions

In this work, we examined the possible future development of paralleled VSC-HVDC and AC links to transmit power generated from large geothermal sources in the far north east of South Australia to Northern New South Wales and the mid-north of South Australia. A well-established higher-order, small-signal model of DB-controlled VSC-HVDC links is integrated with the extended simplified South Eastern (SE) Australian power system model to form a large, interconnected AC/DC parallel operated system in a MATLAB simulation environment. The major stability issue in such a system is the lightly damped inter-area oscillations.

To enhance the damping stability of the investigated system, two forms of stabilization were examined: (i) generator power system stabilizers (PSS) fitted to the synchronous machines, which are used to convert geothermal energy to electrical power; and (ii) power oscillation damping controllers (PODs) fitted to the VSC-HVDC link. In the case of the PODs, two types of stabilizing input signals are considered: (i) local signals such as power flow in adjacent AC lines and (ii) wide-area signals such as bus voltage angles at key nodes in the various regions of the system. The frequency domain approach based on eigenvalue analysis and time domain simulations considering various operating points were performed in this study to demonstrate the effectiveness of the developed supplementary control schemes. We thus conclude that the small-signal rotor -angle stability of the interconnected AC/DC system was significantly enhanced by employing the designed damping controllers.

Author Contributions: Conceptualization, L.W. and M.N.; methodology, N.E.; software, L.W.; validation, L.W., M.N. and N.E.; formal analysis, L.W.; investigation, N.E.; resources, M.N.; data curation, L.W.; writing—original draft preparation, M.N.; writing—review and editing, N.E.; visualization, M.N.; supervision, L.W.; project administration, N.E.; funding acquisition, M.N. All authors have read and agreed to the published version of the manuscript.

Funding: This research received no external funding.

Institutional Review Board Statement: Not applicable.

Informed Consent Statement: Not applicable.

Acknowledgments: The authors would like to acknowledge the support provided by the China Scholarship Council (CSC)-University of Adelaide (UA) Joint Postgraduate Scholarships.

Conflicts of Interest: The authors declare no conflict of interest.

Appendix A

Appendix A.1 Algorithm for Interconnection of Sub-Systems

After the sub-systems are transformed into their state space form, a single state space model can be obtained by grouping these sub-models appropriately. Although this has been performed previously in [14,45,46], it was based on the matrix substitution technique. The interconnection algorithm employed in this paper is given below.

Figure A1 shows a set of state space equations and algebraic equations to demonstrate the sub-modular interconnection approach.

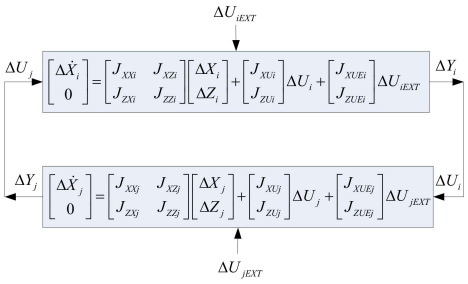

Figure A1. Demonstration of sub-modular interconnection.

The state space equations of two separate systems i and j are defined by:

$$\begin{bmatrix} \Delta\dot{X}_i \\ 0 \end{bmatrix} = \begin{bmatrix} J_{XXi} & J_{XZi} \\ J_{ZXi} & J_{ZZi} \end{bmatrix} \begin{bmatrix} \Delta X_i \\ \Delta Z_i \end{bmatrix} + \begin{bmatrix} J_{XUi} \\ J_{ZUi} \end{bmatrix} \Delta U_i + \begin{bmatrix} J_{XUEi} \\ J_{ZUEi} \end{bmatrix} \Delta U_{iEXT} \tag{A1}$$

$$\begin{bmatrix} \Delta\dot{X}_j \\ 0 \end{bmatrix} = \begin{bmatrix} J_{XXj} & J_{XZj} \\ J_{ZXj} & J_{ZZj} \end{bmatrix} \begin{bmatrix} \Delta X_j \\ \Delta Z_j \end{bmatrix} + \begin{bmatrix} J_{XUj} \\ J_{ZUj} \end{bmatrix} \Delta U_j + \begin{bmatrix} J_{XUEj} \\ J_{ZUEj} \end{bmatrix} \Delta U_{jEXT} \tag{A2}$$

$$\begin{aligned} \Delta Y_i &= J_{YXi}\Delta X_i + J_{YZi}\Delta Z_i + J_{YUi}\Delta U_i; \\ \Delta U_j &= \Delta Y_i; \end{aligned} \tag{A3}$$

$$\begin{aligned} \Delta Y_j &= J_{YXj}\Delta X_j + J_{YZj}\Delta Z_j + J_{YUj}\Delta U_j; \\ \Delta U_i &= \Delta Y_j; \end{aligned} \tag{A4}$$

The above equations can be written as:

$$\begin{bmatrix} \Delta\dot{X}_i \\ 0 \end{bmatrix} = \begin{bmatrix} J_{XXi} & J_{XZi} \\ J_{ZXi} & J_{ZZi} \end{bmatrix} \begin{bmatrix} \Delta X_i \\ \Delta Z_i \end{bmatrix} + \begin{bmatrix} J_{XUi} \\ J_{ZUi} \end{bmatrix} \Delta U_i + \begin{bmatrix} J_{XUEi} \\ J_{ZUEi} \end{bmatrix} \Delta U_{iEXT} \tag{A5}$$

$$0 = \begin{bmatrix} J_{YXi} & J_{YZi} \end{bmatrix} \begin{bmatrix} \Delta X_i \\ \Delta Z_i \end{bmatrix} + [J_{YUi}]\Delta U_i - [\Pi]\Delta Y_i \tag{A6}$$

$$\begin{bmatrix} \Delta\dot{X}_j \\ 0 \end{bmatrix} = \begin{bmatrix} J_{XXj} & J_{XZj} \\ J_{ZXj} & J_{ZZj} \end{bmatrix} \begin{bmatrix} \Delta X_j \\ \Delta Z_j \end{bmatrix} + \begin{bmatrix} J_{XUj} \\ J_{ZUj} \end{bmatrix} \Delta U_j + \begin{bmatrix} J_{XUEj} \\ J_{ZUEj} \end{bmatrix} \Delta U_{jEXT} \tag{A7}$$

$$0 = \begin{bmatrix} J_{YXj} & J_{YZj} \end{bmatrix} \begin{bmatrix} \Delta X_j \\ \Delta Z_j \end{bmatrix} + \left[J_{YUj}\right]\Delta U_j - [\Pi]\Delta Y_j \tag{A8}$$

$$0 = [\Pi]\Delta U_j - [\Pi]\Delta Y_i \tag{A9}$$

$$0 = [\Pi]\Delta U_i - [\Pi]\Delta Y_j \tag{A10}$$

Then, they can be combined in a matrix form as:

$$\begin{bmatrix} \Delta\dot{x}_i \\ \Delta\dot{x}_j \\ 0 \\ 0 \\ 0 \\ 0 \\ 0 \\ 0 \end{bmatrix} = \overbrace{\left[\begin{array}{cc:cccccc} J_{XXi} & 0 & J_{XZi} & 0 & 0 & 0 & J_{XUi} & 0 \\ 0 & J_{XXj} & 0 & J_{XZj} & 0 & 0 & 0 & J_{XUj} \\ \hdashline J_{ZXi} & 0 & J_{ZZi} & 0 & 0 & 0 & J_{ZUi} & 0 \\ 0 & J_{ZXj} & 0 & J_{ZZj} & 0 & 0 & 0 & J_{ZUj} \\ J_{YXi} & 0 & J_{YZi} & 0 & -\Pi & 0 & J_{YUi} & 0 \\ 0 & J_{YXj} & 0 & J_{YZj} & 0 & -\Pi & 0 & J_{YUj} \\ 0 & 0 & 0 & 0 & -\Pi & 0 & 0 & \Pi \\ 0 & 0 & 0 & 0 & 0 & -\Pi & \Pi & 0 \end{array}\right]}^{J_{XX(C)}\quad J_{XZ(C)}} \begin{bmatrix} \Delta X_i \\ \Delta X_j \\ \Delta Z_i \\ \Delta Z_j \\ \Delta Y_i \\ \Delta Y_j \\ \Delta U_i \\ \Delta U_j \end{bmatrix} + \overbrace{\left[\begin{array}{cc} J_{XUei} & 0 \\ 0 & J_{XUej} \\ \hdashline J_{ZUei} & 0 \\ 0 & J_{ZUej} \\ J_{YUei} & 0 \\ 0 & J_{YUei} \\ J_{UUei} & 0 \\ 0 & J_{UUei} \end{array}\right]}^{J_{XUE(C)}} \begin{bmatrix} \Delta u_{iext} & 0 \\ 0 & \Delta u_{jext} \end{bmatrix} \tag{A11}$$

$$\underbrace{\qquad}_{J_{ZX(C)}} \qquad \underbrace{\qquad\qquad\qquad\qquad}_{J_{ZZ(C)}} \qquad \underbrace{\qquad}_{J_{ZUE(C)}}$$

and

$$\begin{aligned} \Delta X_{(C)} &= \begin{bmatrix} \Delta X_i & \Delta X_j \end{bmatrix}^T; \\ \Delta Z_{(C)} &= \begin{bmatrix} \Delta Z_i & \Delta Z_j & \Delta Y_i & \Delta Y_j & \Delta U_i & \Delta U_j \end{bmatrix}^T; \end{aligned}$$

This allows us to obtain a single set of equations from two separate sets of equations. Hence, using this block interconnection approach, all sub-components of the system can be mathematically grouped together.

Appendix A.2 Residue analysis of the System

Table A1. Residue analysis of the system.

Mode	Rectifier Side Power Reference Input																			
	Local Signal				Wide Area Signal															
	ΔPL_{12}		ΔPL_{34}		$\Delta\omega_{BS}$		$\Delta\delta_{BS}$		$\Delta\omega_{BM}$		$\Delta\delta_{BM}$		$\Delta\omega_{BA}$		$\Delta\delta_{BA}$		$\Delta\omega_{BI}$		$\Delta\delta_{BI}$	
	Mag	Ang	Mag	Ang	Mag	Ang	Mag	Ang	Mag	Ang	Mag	Ang	Mag	Ang	Mag	Ang	Mag	Ang	Mag	Ang
I40	1.8×10^{-8}	7.977	1.92×10^{-7}	40.21	2.67×10^{-11}	−85.879	2.14×10^{-9}	4.4266	1.26×10^{-10}	−18.249	1.01×10^{-8}	72.057	2.14×10^{-10}	−30.191	1.71×10^{-8}	60.114	3.39×10^{-10}	−54.016	2.68×10^{-8}	30.107
I35	5.56×10^{-8}	18.854	2.04×10^{-7}	−54.671	7.46×10^{-11}	−70.941	6.81×10^{-9}	18.144	2.24×10^{-10}	4.7301	2.04×10^{-8}	−86.186	1.45×10^{-10}	78.327	1.32×10^{-8}	−12.588	4.03×10^{-10}	28.82	3.68×10^{-8}	−67.306
I25	9.15×10^{-8}	25.811	4.01×10^{-7}	52.865	8.67×10^{-11}	−60.239	1.19×10^{-9}	26.285	8.86×10^{-10}	−53.842	1.21×10^{-8}	32.683	9.05×10^{-10}	5.6807	1.24×10^{-8}	−87.795	7.60×10^{-10}	−24.096	1.02×10^{-8}	57.854
I15	0.0045244	−3.4094	0.0066914	89.684	3.31×10^{-6}	−89.091	0.0006068	−2.3052	7.99×10^{-6}	−55.874	0.0014634	30.911	2.01×10^{-5}	−24.17	0.0036817	62.615	2.76×10^{-5}	−14.135	0.005093	70.661

References

1. AEMO. AEMO Australian Energy Market Operator. Available online: www.aemo.com.au (accessed on 1 March 2022).
2. Nguyen, M.H.; Eghbal, M.; Saha, T.K.; Modi, N. Investigation of Oscillation Damping for connecting remote generators to a large power system. In Proceedings of the Innovative Smart Grid Technologies Asia (ISGT), Perth, WA, Australia, 13–16 November 2011; pp. 1–8.
3. Huong, M.N.; Saha, T.K.; Eghbal, M. Investigation on the impact of hybrid multi-terminal HVDC system combining LCC and VSC technologies using system identification. In Proceedings of the Universities Power Engineering Conference (AUPEC), 2012 22nd Australasian, Bali, Indonesia, 26–29 September 2012; pp. 1–6.
4. Nguyen, M.H.; Saha, T.K.; Eghbal, M. Hybrid multi-terminal LCC HVDC with a VSC Converter: A case study of Simplified South East Australian system. In Proceedings of the Power and Energy Society General Meeting, San Diego, CA, USA, 22–26 July 2012; pp. 1–8.
5. de Silva, R.; Robbie, A. *Network Extensions to Remote Areas: Part 2–Innamincka Case Study*; Power Systems Consultants Australia Pty Ltd.: Melbourne, Australia, 2009.
6. Povh, D.; Retzmann, D.; Teltsch, E.; Kerin, U.; Mihalic, R. Advantages of large ac/dc system interconnections. *Rep. B4-304 CIGRE Sess.* **2006**, 1–10.
7. Pan, J.; Nuqui, R.; Srivastava, K.; Jonsson, T.; Holmberg, P.; Hafner, Y.-J. AC grid with embedded VSC-HVDC for secure and efficient power delivery. In Proceedings of the 2008 IEEE Energy 2030 Conference, Atlanta, GA, USA, 17–18 November 2008; pp. 1–6.
8. Latorre, H.F.; Ghandhari, M.; Soder, L. Use of local and remote information in POD control of a VSC-HVdc. In Proceedings of the PowerTech, Bucharest, Romania, 28 June–2 July 2009; pp. 1–6.
9. Weixing, L.; Ooi, B.T. Simultaneous inter-area decoupling and local area damping by voltage source HVDC. In Proceedings of the 2001 IEEE Power Engineering Society Winter Meeting, Columbus, OH, USA, 28 January–1 February 2001; Volume 3, pp. 1079–1084.
10. Piwko, R.J.; Larsen, E.V. HVDC System Control for Damping of Subsynchronous Oscillations. *IEEE Trans. Power Appar. Syst.* **1982**, *PAS-101*, 2203–2211. [CrossRef]
11. Kundur, P. *Power System Stability And Control*; McGraw-Hill: New York, NY, USA, 1994.
12. Vowles, D.J.; Samarasinghe, C.; Gibbard, M.J.; Ancell, G. Effect of wind generation on small-signal stability—A New Zealand Example. In Proceedings of the Power and Energy Society General Meeting—Conversion and Delivery of Electrical Energy in the 21st Century, Pittsburgh, PA, USA, 20–24 July 2008; pp. 1–8.
13. Gibbard, M.J.; Vowles, D.J.; Pourbeik, P. Interactions between, and effectiveness of power system stabilizers and FACTS device stabilizers in multimachine systems. *IEEE Trans. Power Syst.* **2000**, *2*, 1532.
14. Chang, Y. Design of HVDC and SVC Coordinate Damping Controller Based on Wide Area Signal. *Int. J. Emerg. Electr. Power Syst.* **2006**, *7*, 6. [CrossRef]
15. Yong, C.; Zheng, X.; Gaihong, C.; Jiani, X. A novel SVC supplementary controller based on wide area signals. In Proceedings of the Power Engineering Society General Meeting, Montreal, QC, Canada, 18–22 June 2006; p. 7.

16. Uhlen, K.; Vanfretti, L.; de Oliveira, M.; Leirbukt, A.; Aarstrand, V.H.; Gjerde, J.O. Wide-Area Power Oscillation Damper implementation and testing in the Norwegian transmission network. In Proceedings of the Power and Energy Society General Meeting, San Diego, CA, USA, 22–26 July 2012; pp. 1–7.
17. Ying, J.-H.; Duchen, H.; Linden, K.; Hyttinen, M.; de Toledo, P.F.; Tulkiewicz, T.; Skytt, A.K.; Bjorklund, H. Improvement of subsynchronous torsional damping using VSC HVDC. In Proceedings of the International Conference on Power System Technology, Kunming, China, 13–17 October 2002; Volume 2, pp. 998–1003.
18. Chao, Z.; Zhou, X.; Ruomei, L. Dynamic Modeling and Transient Simulation for VSC based HVDC in Multi-Machine System. In Proceedings of the 2006 International Conference on Power System Technology, Chongqing, China, 22–26 October 2006; pp. 1–7.
19. Latorre, H.F.; Ghandhari, M.; Soder, L. Control of a VSC-HVDC Operating in Parallel with AC Transmission Lines. In Proceedings of the Transmission & Distribution Conference and Exposition: Latin America, 2006. TDC '06. IEEE/PES, Caracas, Venezuela, 15–18 August 2006; pp. 1–5.
20. Latorre, H.F.; Ghandhari, M. Improvement of voltage stability by using VSC-HVdc. In Proceedings of the Transmission & Distribution Conference & Exposition: Asia and Pacific, Seoul, Korea, 26–30 October 2009; pp. 1–4.
21. Preece, R.; Milanovic, J.V.; Almutairi, A.M.; Marjanovic, O. Damping of Inter-Area Oscillations in Mixed AC/DC Networks Using WAMS Based Supplementary Controller. *IEEE Trans. Power Syst.* **2013**, *28*, 1160–1169. [CrossRef]
22. Domínguez-García, J.L.; Gomis-Bellmunt, O.; Bianchi, F.D.; Sumper, A. Power oscillation damping supported by wind power: A review. *Renew. Sustain. Energy Rev.* **2012**, *16*, 4994–5006. [CrossRef]
23. Heniche, A.; Kamwa, I. Assessment of Two Methods to Select Wide-Area Signals for Power System Damping Control. *IEEE Trans. Power Syst.* **2008**, *23*, 572–581. [CrossRef]
24. Modi, N.; Lloyd, M.; Saha, T.K. Wide-area signal selection for power system damping controller. In Proceedings of the Universities Power Engineering Conference (AUPEC), 2011 21st Australasian, Brisbane, QLD, Australia, 25–28 September 2011; pp. 1–6.
25. Pourbeik, P.; Gibbard, M.J. Tuning of SVC stabilisers for the damping of inter-area modes of rotor oscillation. In Proceedings of the Australasian Universities Power Engineering Conference, Nedlands, WA, Australia, 27–29 September 1995.
26. Gibbard, M. *Tuning of Power System Stabilizaers(PSS)*; School of Electrical and Electronic Engineering Notes, The University of Adelaide: Adelaide, Australia, 1998.
27. Vowles, D.J. *Tuning of Stabilizers for FACTS Devices*; School of Electrical and Electronic Engineering Notes, The University of Adelaide: Adelaide, Australia, 1998.
28. Gibbard, M. Co-ordinated design of multimachine power system stabilisers based on damping torque concepts. *IEE Proc. C (Gener. Transm. Distrib.)* **1988**, *135*, 276–284. [CrossRef]
29. Gibbard, M.J. Robust design of fixed-parameter power system stabilisers over a wide range of operating conditions. *IEEE Trans. Power Syst.* **1991**, *6*, 794–800. [CrossRef]
30. Gibbard, M.J.; Martins, N.; Sanchez-Gasca, J.J.; Uchida, N.; Vittal, V.; Wang, L. Recent applications of linear analysis techniques. *IEEE Trans. Power Syst.* **2001**, *16*, 154–162. [CrossRef]
31. Spallarossa, C.; Pipelzadeh, Y.; Chaudhuri, B.; Green, T. Assessment of disturbance propagation between AC grids through VSC HVDC links using reduced Great Britain model. In Proceedings of the 10th IET International Conference on AC and DC Power Transmission (ACDC 2012), Birmingham, UK, 4–5 December 2012.
32. Wang, J.; Fu, C.; Zhang, Y. Design of WAMS-Based Multiple HVDC Damping Control System. *IEEE Trans. Smart Grid* **2011**, *2*, 363–374. [CrossRef]
33. Zhang, J.; Chung, C.Y.; Zhang, S.; Han, Y. Practical Wide Area Damping Controller Design Based on Ambient Signal Analysis. *IEEE Trans. Power Syst.* **2013**, *28*, 1687–1696. [CrossRef]
34. Grainger, W.; Parker, C.; Wright, P. Commissioning a new interconnection between two regions in Australia. *Cigre Electra Magazine*, April 2001; 10–17.
35. Hiley, S. *Redesign of the Blackwall Static Var Compensator Power Oscillation Damper Controller. School of Information Technology and Electrical Engineering*; the University of Queensland: Brisbane, Australia, 2007.
36. Latorre, H.F.; Ghandhari, M.; Söder, L. Active and reactive power control of a VSC-HVdc. *Electr. Power Syst. Res.* **2008**, *78*, 1756–1763. [CrossRef]
37. Vowles, D.J.; Gibbard, M. Simplified 14-Generator Model of the SE Australian Power System. *Univ. Adel. South Aust.* **2014**, *18*, 1–38.
38. Liying, W. Modeling, Control and Stability Analysis of VSC-HVDC links Embedded in a Weak Multi-Machine AC System. Ph.D. Thesis, School of Electrical and Electrinic Engineering, the University of Adelaide, Adelaide, Australia, 2013.
39. China HVDC Transmission, Special Report, ABB PEI Power Engineering International. Available online: https://library.e.abb.com/public/d55e6e1fc25ef3d8c1256f4000370e0e/PT_HVDC_TransmChina.pdf (accessed on 1 March 2022).
40. Yang, F. Study on Parameter Optimization of HDVC PI Controllers. *Power Syst. Technol.* **2006**, *30*, 15–20.
41. Jacobson, B.W.B.; Bahrman, M.P. 500 kV VSC Transmission System for lines and cables. In Proceedings of the 2012 San Francisco Colloquium, San Francisco, CA, USA; 2012.
42. Karawita, C.; Annakkage, U.D. A Hybrid Network Model for Small Signal Stability Analysis of Power Systems. *IEEE Trans. Power Syst.* **2010**, *25*, 443–451. [CrossRef]
43. Gibbard, M.J.; Vowles, D.J. Reconciliation of methods of compensation for PSSs in multimachine systems. *IEEE Trans. Power Syst.* **2004**, *19*, 463–472. [CrossRef]

44. Sadikovic, R.; Andersson, G.; Korba, P. Damping controller design for power system oscillations. *Intell. Autom. Soft Comput.* **2006**, *12*, 51–62. [CrossRef]
45. Podrucky, S. *Small Signal Modeling of Resonant Controlled VSC Systems*; University of Toronto: Toronto, QC, Canada, 2009.
46. Rault, P.; Colas, F.; Guillaud, X.; Nguefeu, S. Method for small signal stability analysis of VSC-MTDC grids. In Proceedings of the Power and Energy Society General Meeting, San Diego, CA, USA, 22–26 July 2012; pp. 1–7.